Supplementary Material

Structure of BIRC7–E2 ubiquitin conjugate reveals the mechanism of ubiquitin transfer by a RING dimer

Hao Dou, Lori Buetow, Gary J. Sibbet, Kenneth Cameron and Danny T. Huang

Table of Contents

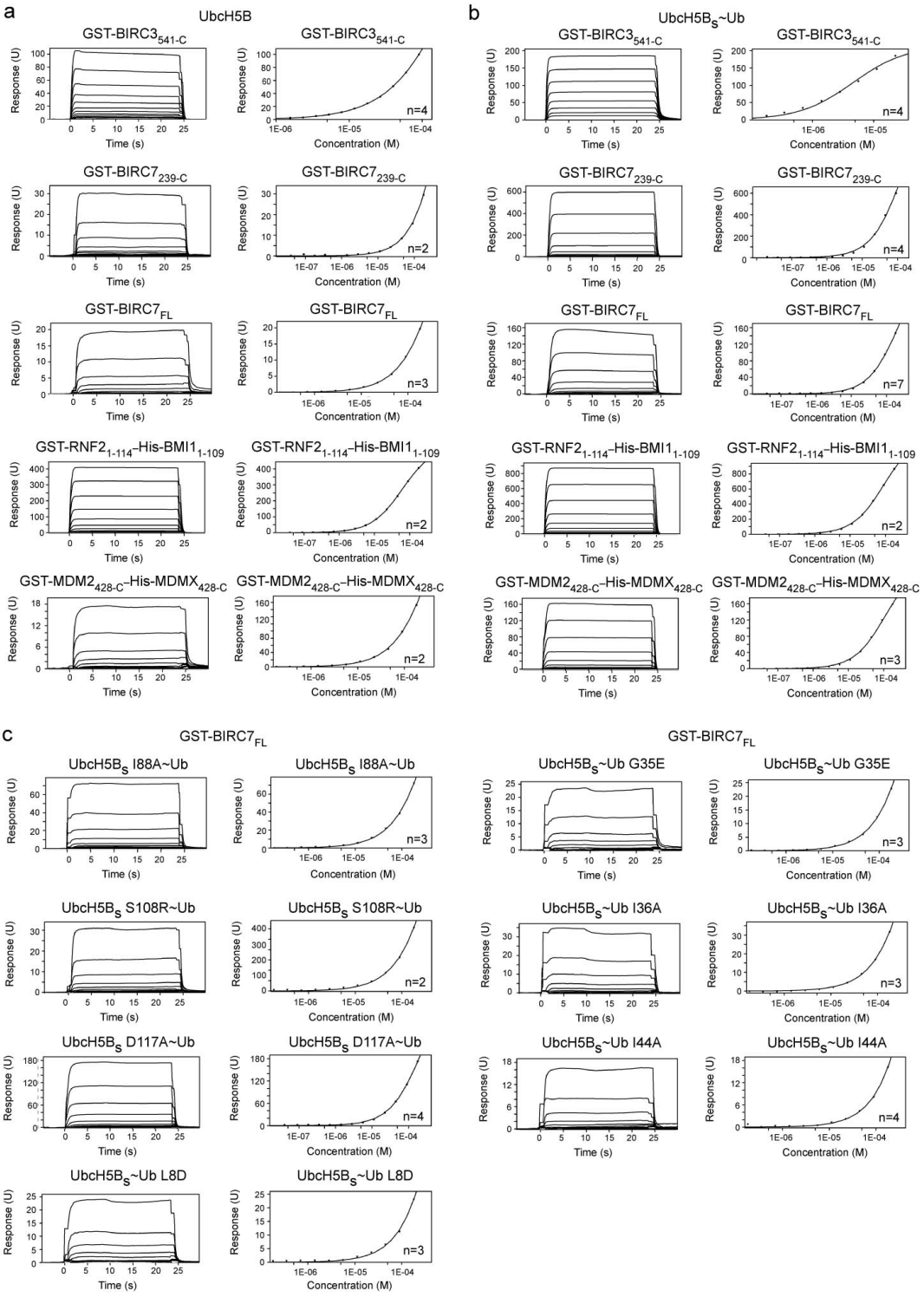
a
UbcH5B
GST-BIRC3541-C
GST-BIRC7239-C
GST-BIRC7FL
GST-RNF2 1-114–His-BMI1 1-109
GST-MDM2 428-C–His-MDMX 428-C
b
UbcH5BS~Ub
c
GST-BIRC7FL
UbcH5BS I88A~Ub
UbcH5BS S108R~Ub
UbcH5BS D117A~Ub
UbcH5BS~Ub L8D
UbcH5BS~Ub G35E
UbcH5BS~Ub I36A
UbcH5BS~Ub I44A
Response (U)
Time (s)
Concentration (M)
n=2
n=3
n=4
n=7

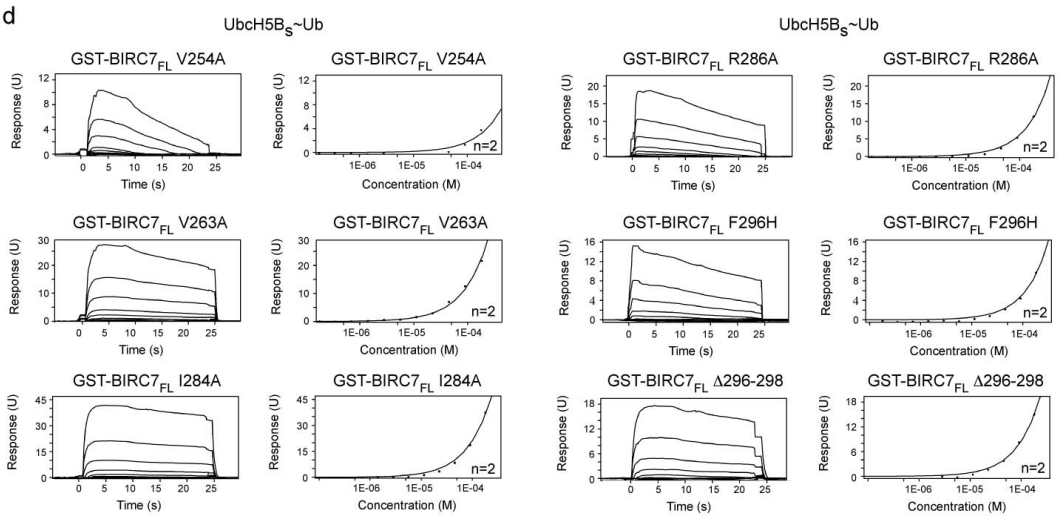

Supplementary Figure 1 Surface plasmon resonance analyses of UbcH5B and UbcH5B$_S$~Ub variants binding to dimeric RING variants. Representative sensorgrams (left) and binding curves (right) for GST-RING E3 variants with UbcH5B (**a**), UbcH5B$_S$~Ub (**b**), GST-BIRC7$_{FL}$ with UbcH5B$_S$~Ub variants (**c**), GST-BIRC7$_{FL}$ variants with UbcH5B$_S$~Ub (**d**), as indicated. GST-ligands and analytes are indicated above the sensorgrams and binding curves. The number of replicates is indicated in the binding curve.

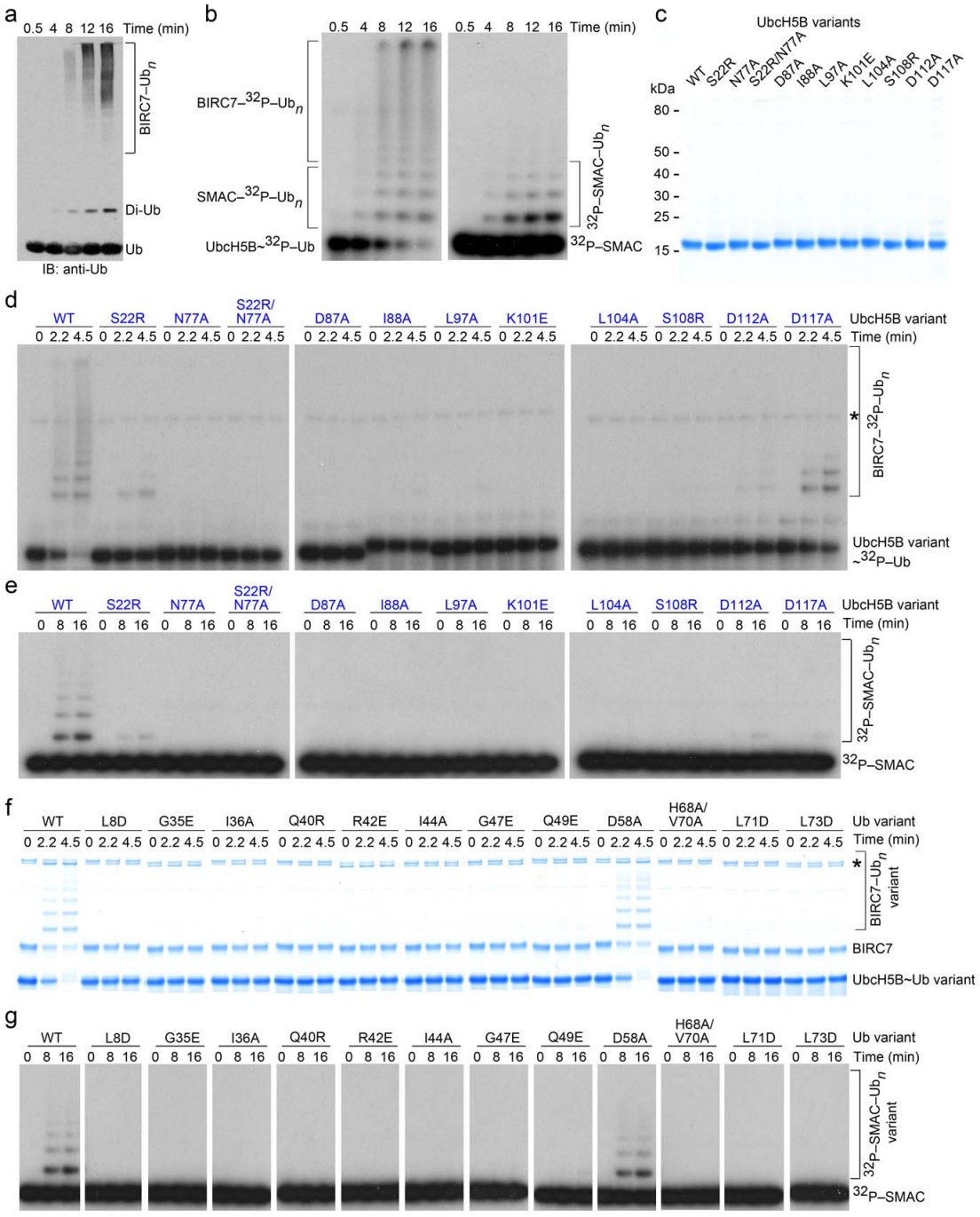

Supplementary Figure 2 Additional *in vitro* ubiquitination assays. (**a**) Autoubiquitination of BIRC7 occurs in di-Ub formation assays. Western blot from *in vitro* di-Ub formation assay with wild-type BIRC7, UbcH5B and Ub under pulse-chase conditions. (**b**) Autoubiquitination of BIRC7 occurs in SMAC-ubiquitination assays. Ub$_n$, Ub chain of length *n*. Left: Non-reduced autoradiogram of SMAC ubiquitination showing the simultaneous disappearance of UbcH5B~^{32}P-Ub and the formation of BIRC7–Ub$_n$ and SMAC–Ub$_n$ over time with wild-type UbcH5B, BIRC7 and ^{32}P-Ub under pulse-chase conditions. Right: Non-reduced autoradiogram showing

the formation of ^{32}P-SMAC–Ub$_n$ over time run under conditions identical to those in the left panel but with ^{32}P-SMAC and unlabeled Ub. (**c**) SDS-PAGE showing 2 μg of purified UbcH5B variants. Molecular weight standard is indicated. (**d**) Non-reduced autoradiograms of pulse-chase reactions showing the simultaneous formation of ^{32}P-Ub products and disappearance of UbcH5B~^{32}P-Ub with full-length BIRC7 and UbcH5B variants over time. An asterisk indicates the E1~Ub band. (**e**) Non-reduced autoradiogram showing the formation of ^{32}P-SMAC–Ub$_n$ over time as in **b** but with UbcH5B variants. (**f**) Non-reduced SDS-PAGE of pulse-chase reactions showing the simultaneous formation of ^{32}P-Ub products and disappearance of UbcH5B~^{32}P-Ub with full-length BIRC7, UbcH5B and Ub variants over time. (**g**) Non-reduced autoradiogram showing the formation of ^{32}P-SMAC–Ub$_n$ over time as in **b** but with Ub variants.

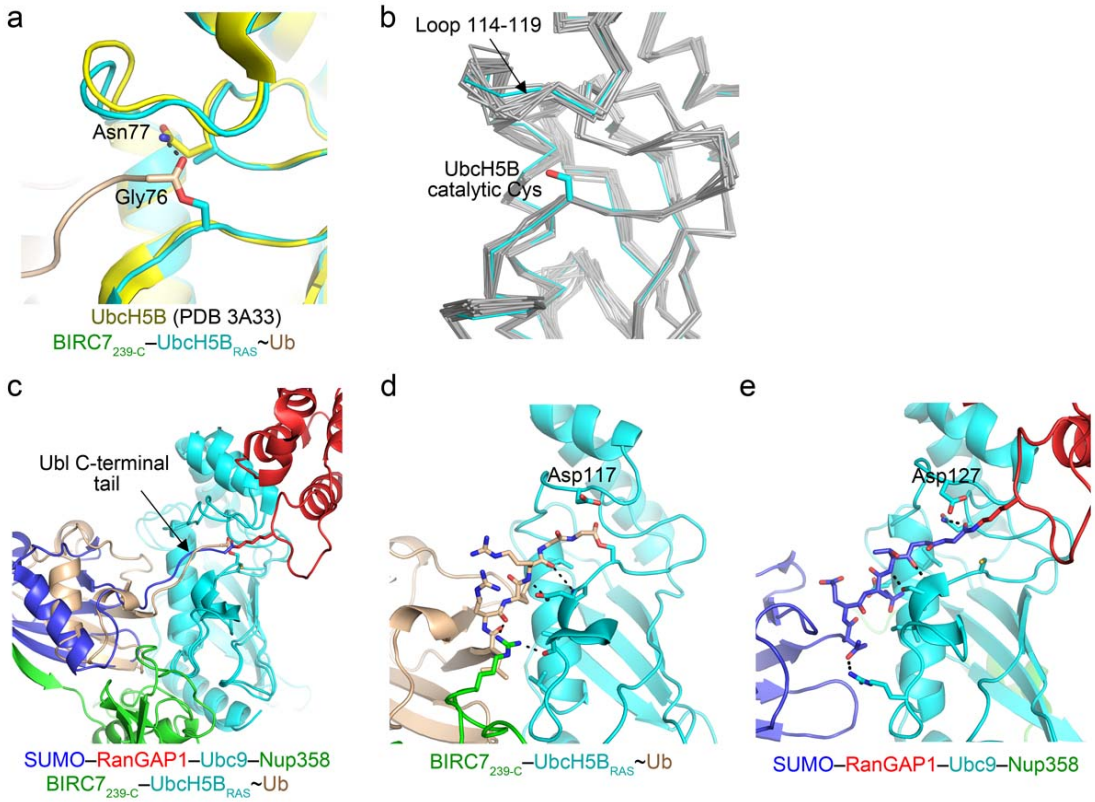

Supplementary Figure 3 E2–Ub tail interactions. (**a**) Close-up view of the active site from a structural alignment of UbcH5B from PDB 3A33 (colored yellow) and $BIRC7_{239–C}$–$UbcH5B_{RAS}$~Ub (colored cyan). Gly76 and N77A from $BIRC7_{239–C}$–$UbcH5B_{RAS}$~Ub and Asn77 from PDB 3A33 are shown as sticks. (**b**) Movement of UbcH5B loop (114-119). Ribbon diagrams of structural alignments of the Cα atoms of UbcH5B from $BIRC7_{239–C}$–$UbcH5B_{RAS}$~Ub (colored cyan) with available structures of UbcH5B variants (conjugated and unconjugated) from the Protein Data Bank in grey. The catalytic Cys is shown in sticks. (**c-e**) Similar E2–Ubl tail interactions. (**c**) Structural alignment of UbcH5B from our structure with Ubc9 in the post-conjugation SUMO–RanGAP1–Ubc9–Nup358 complex structure (PDB 1Z5S[1]). E2s are colored cyan, E3s green, Ub wheat, SUMO blue, and RanGAP1 red. (**d**) Close-up view of the Ub tail–UbcH5B interactions in $BIRC7_{239–C}$–$UbcH5B_{RAS}$~Ub. (**e**) Close-up view of the SUMO tail–Ubc9 interactions in SUMO–RanGAP1–Ubc9–Nup358. For **d** and **e**, atoms are colored as in **Fig. 2**.

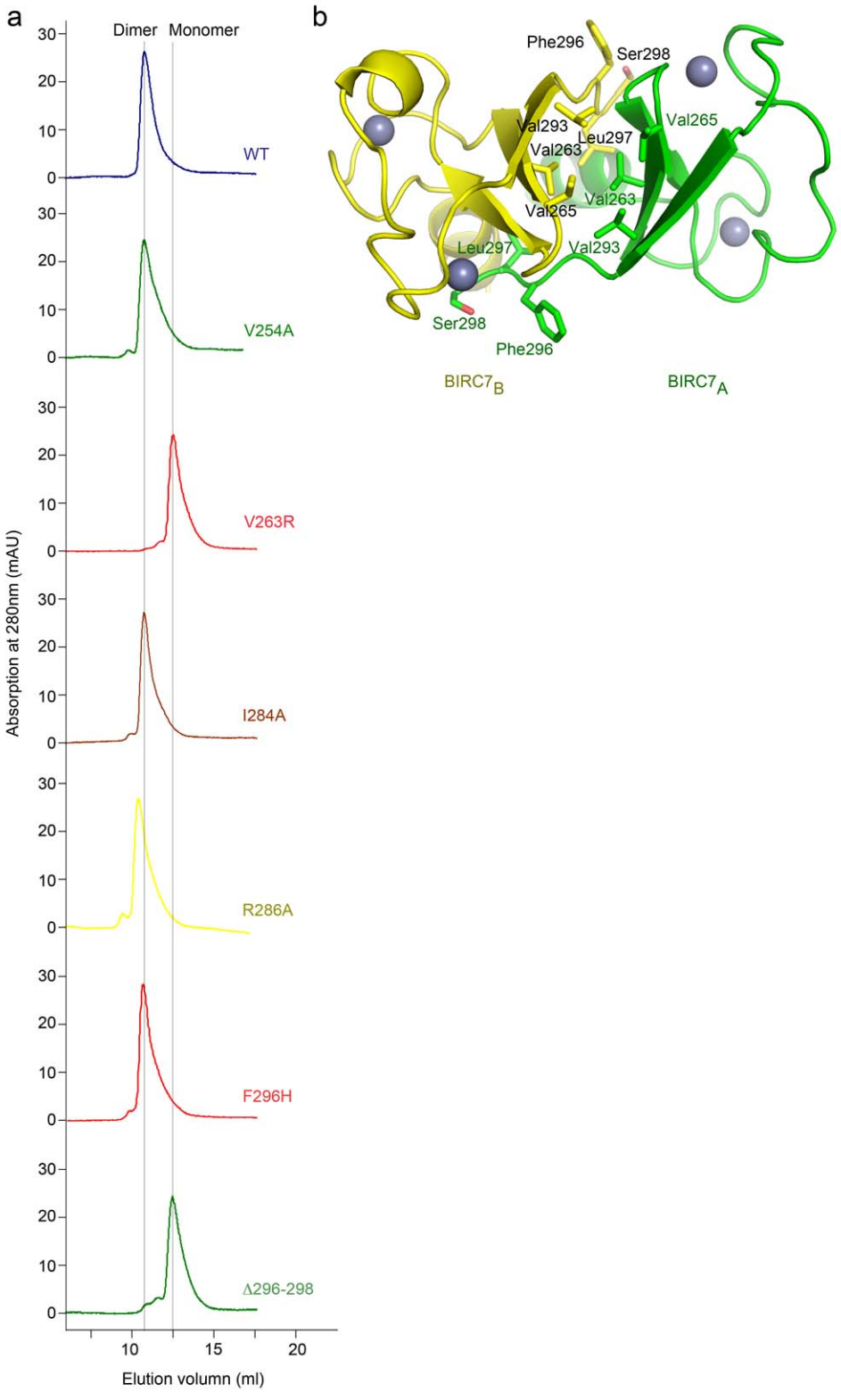

Supplementary Figure 4 BIRC7 dimerization. (**a**) Gel filtration chromatograms of full-length BIRC7 variants. Purified BIRC7 variants (120 μg) were passed over an analytical Superdex 75 10/300 (GE Healthcare). (**b**) Close-up view of the BIRC7 RING–RING dimerization interface in $BIRC7_{239–C}$–$UbcH5B_{RAS}$~Ub complex.

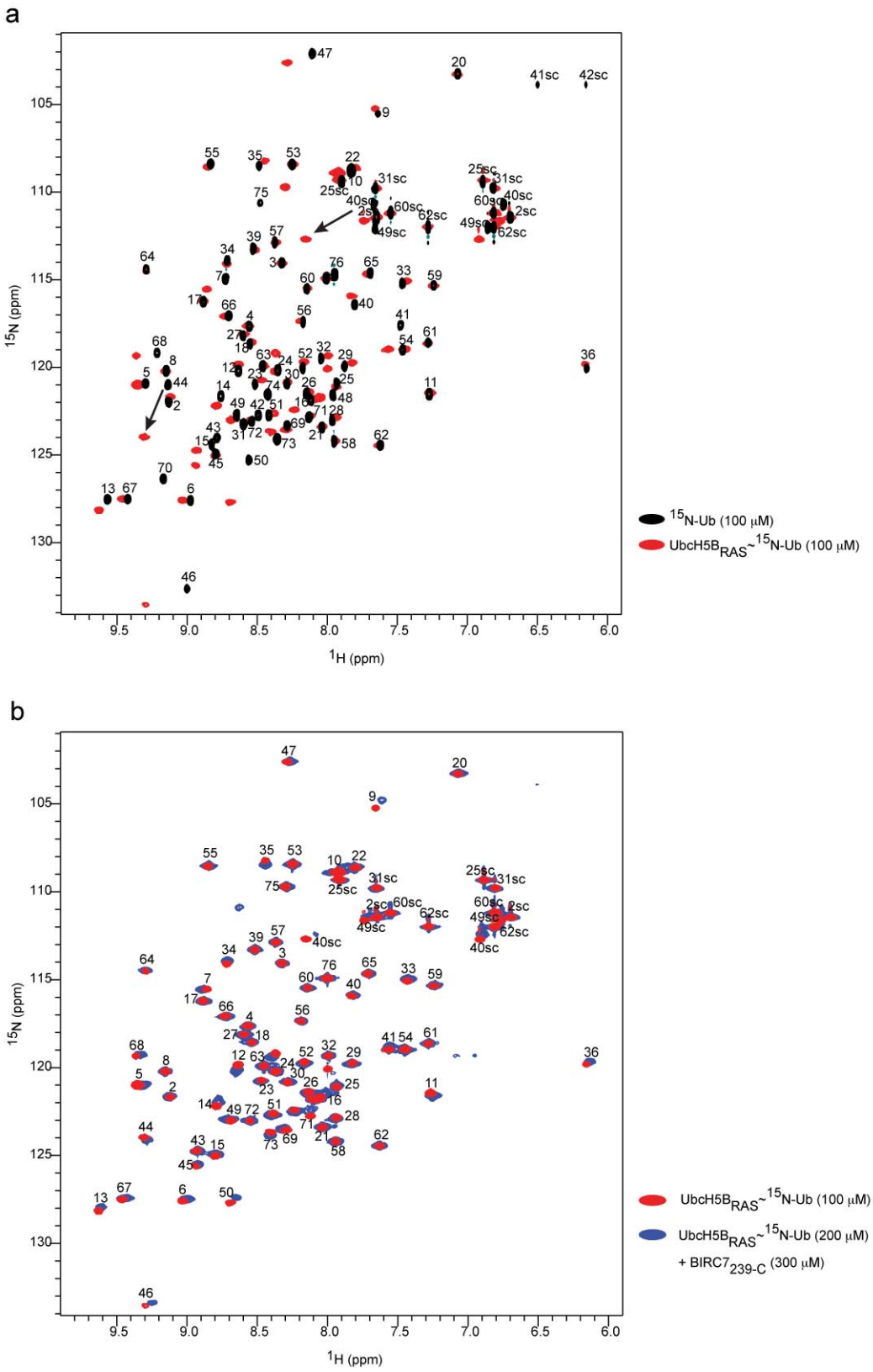
a
^{15}N (ppm)
^{1}H (ppm)
^{15}N-Ub (100 μM)
UbcH5B$_{RAS}$~^{15}N-Ub (100 μM)
b
^{15}N (ppm)
^{1}H (ppm)
UbcH5B$_{RAS}$~^{15}N-Ub (100 μM)
UbcH5B$_{RAS}$~^{15}N-Ub (200 μM)
+ BIRC7$_{239-C}$ (300 μM)

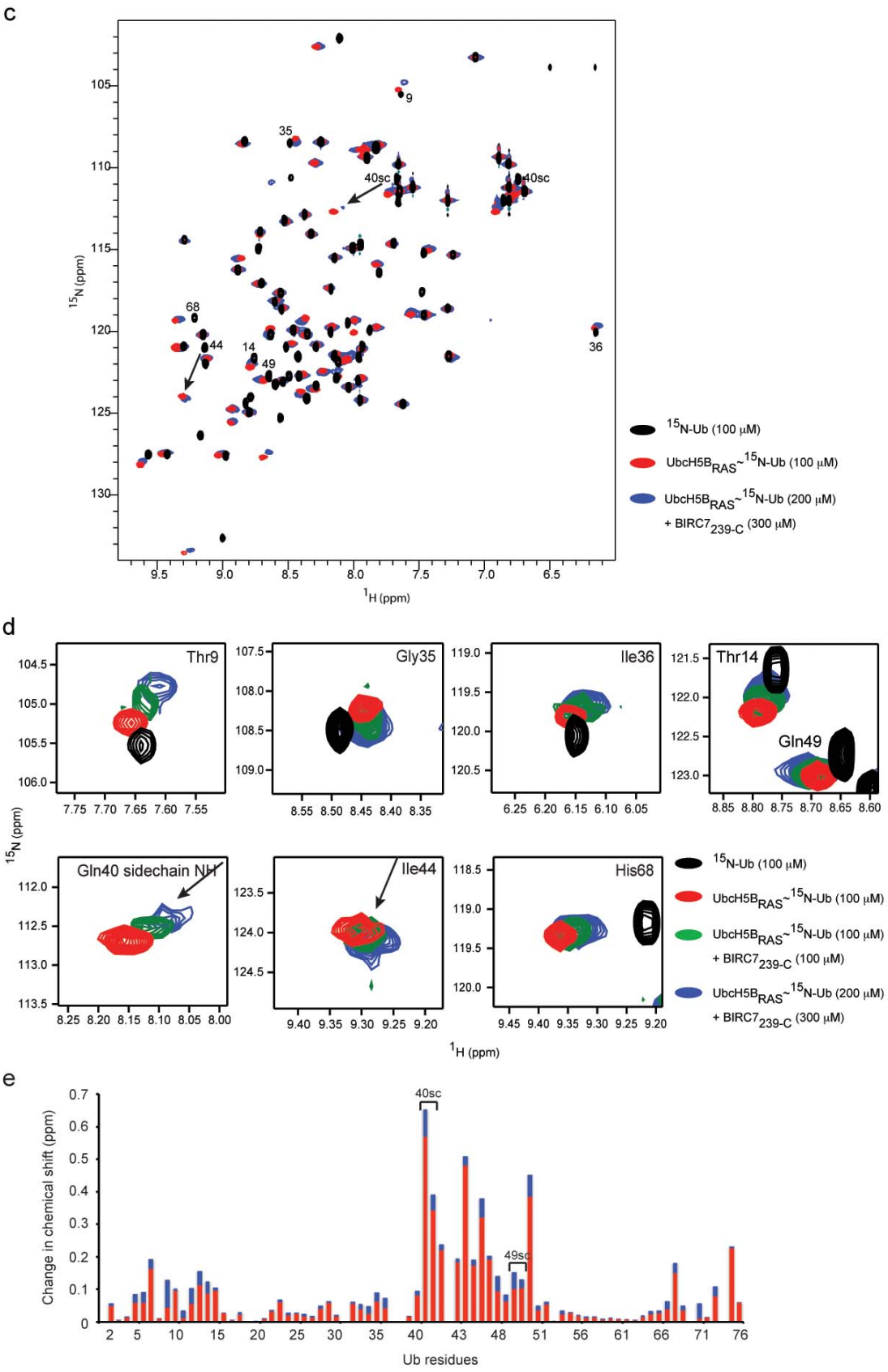

Supplementary Figure 5 Mapping of Ub interactions by NMR. (**a**) Chemical shift perturbation data for Ub in UbcH5B$_{RAS}$~Ub interactions. ^{1}H–^{15}N HSQC spectra for

^{15}N-Ub alone (black) and in the covalent UbcH5B$_{RAS}$~^{15}N-Ub complex (red). Numbers indicate Ub residues in ^{15}N-Ub alone. (**b**) Chemical shift perturbation data for Ub in BIRC7–UbcH5B~Ub interactions. ^{1}H–^{15}N-HSQC spectra for UbcH5B$_{RAS}$~^{15}N-Ub in the absence (red) and presence (blue) of BIRC7$_{239–C}$. Numbers indicate Ub residues in UbcH5B$_{RAS}$~^{15}N-Ub complex. (**c**) ^{1}H–^{15}N-HSQC spectra for ^{15}N-Ub alone (black), UbcH5B$_{RAS}$~^{15}N-Ub (red) and UbcH5B$_{RAS}$~^{15}N-Ub in the presence of BIRC7$_{239–C}$ (blue). (**d**) Expanded regions of the ^{1}H–^{15}N HSQC spectra for Ub alone (100 μM, black), in the covalent UbcH5B$_{RAS}$~Ub complex (100 μM, red), and in the covalent UbcH5B$_{RAS}$~Ub complex (100 μM) with BIRC7$_{239–C}$ (100 μM, green) and in the covalent UbcH5B$_{RAS}$~Ub complex (200 μM) with BIRC7$_{239–C}$ (300 μM, blue). (**e**) Changes in chemical shift per residue of ^{15}N-Ub following covalent linkage to UbcH5B$_{RAS}$ (red) and subsequent addition of 1.5-fold molar excess of BIRC7$_{239–C}$ (blue) determined by ^{1}H–^{15}N HSQC NMR. Changes were calculated according to the equation $[(0.15\ \delta_N)^2 + \delta_H{}^2]^{1/2}$. sc indicates a perturbation in a sidechain NH group. Arrows indicate shift in peaks.

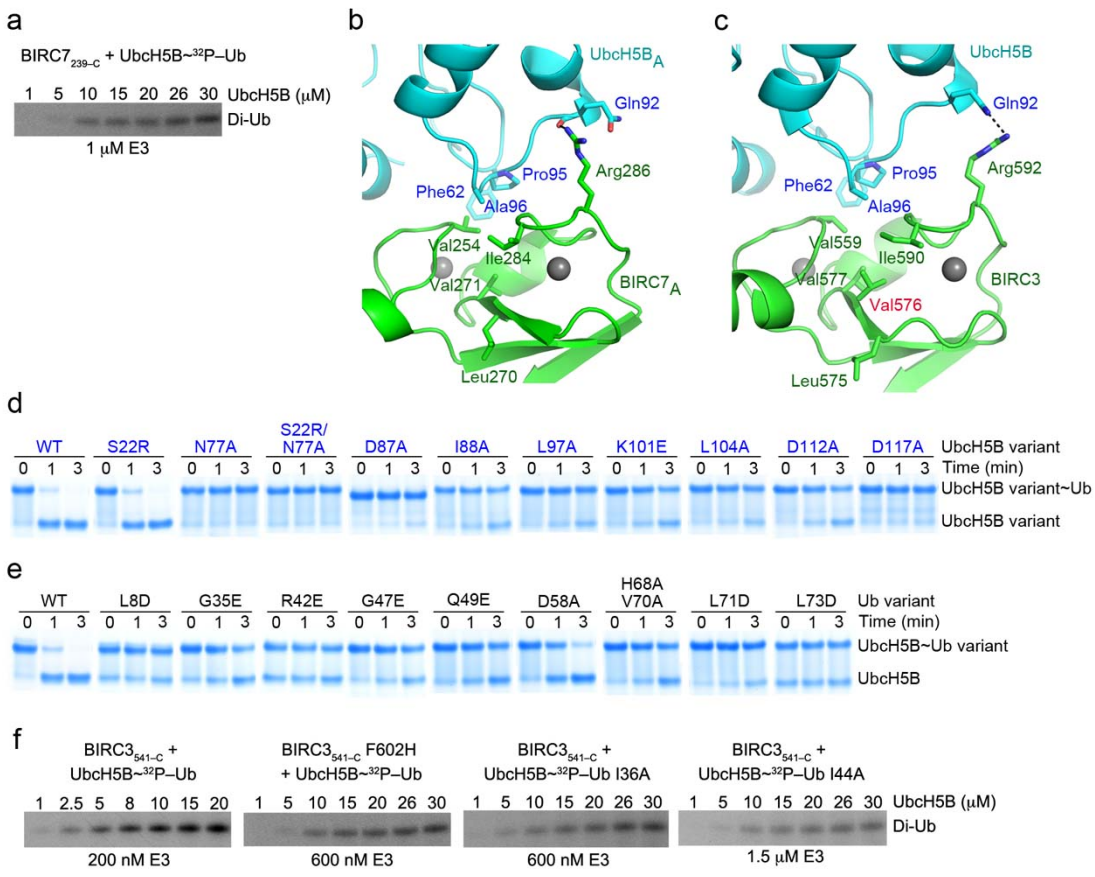

Supplementary Figure 6 Effects of BIRC3, UbcH5B and Ub mutations on ubiquitination activity. (**a**) Single turnover kinetics of di-Ub formation catalyzed by $BIRC7_{239–C}$. UbcH5B was charged with ^{32}P-Ub followed by addition of apyrase and EDTA to stop E1-catalyzed reaction. Various UbcH5B~^{32}P-Ub concentrations were chased with a molar excess of His-Ub in the presence of $BIRC7_{239–C}$. A representative reduced autoradiogram of di-Ub formation is shown. (**b**) Close-up of $BIRC7_A$–$UbcH5B_A$ interactions. (**c**) Close-up of BIRC3–UbcH5B interactions in PDB 3EB6[2]. **b,c** are colored as in **Figs. 1** and **2**. (**d**) Non-reduced SDS-PAGE of pulse-chase reactions showing the disappearance of UbcH5B~Ub with $BIRC3_{541–C}$, L-lysine, and UbcH5B variants over time. (**e**) As in **d** but with Ub variants. (**f**) Single turnover kinetics of di-Ub formation catalyzed by $BIRC3_{239–C}$, UbcH5B and Ub variants. Reactions were performed as in **a**. Representative reduced autoradiograms of di-Ub formation are shown. Final UbcH5B and E3 concentrations are indicated in **a** and **f**.

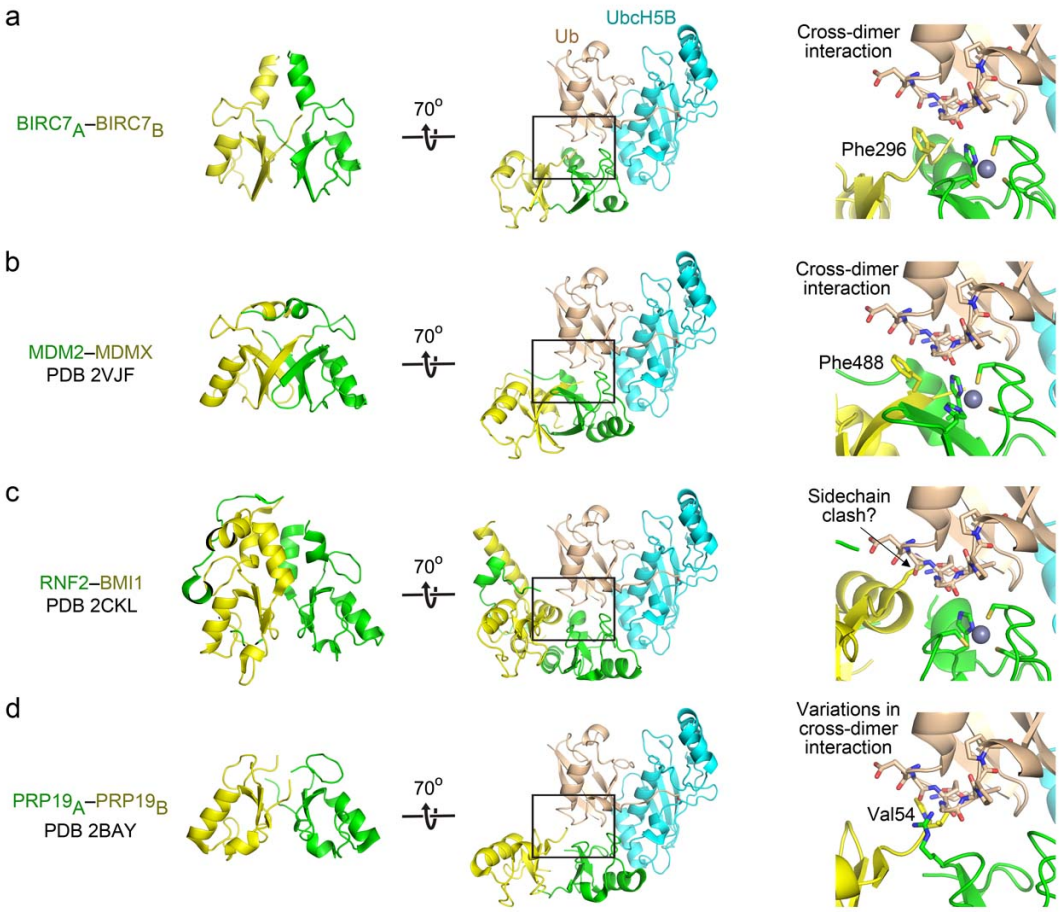

Supplementary Figure 7 Models of dimeric E3–UbcH5B~Ub complexes. (**a**) Left: BIRC7 dimer portion from $BIRC7_{239–C}$–$UbcH5B_{RAS}$~Ub. Middle: BIRC7 dimer–$UbcH5B_A$~Ub_A from $BIRC7_{239–C}$–$UbcH5B_{RAS}$~Ub, rotated 70° from view on left. Right: Close-up view of cross-dimer interactions with Ub from boxed area in middle panel with key residues shown as sticks. (**b-d**) Left: Cartoon representations of E3 dimers generated by structural alignment with the BIRC7 dimer. One subunit is colored green and the second yellow. Middle: Models of UbcH5B~Ub bound to E3 dimers. The green subunits were superimposed onto $BIRC7_A$ to generate these models. Right: Close-up view of E3 dimer interactions with Ub from boxed area of models in the middle panel with key residues shown as sticks. Coloring is as described in **Figs. 1** and **2**.

Supplementary Methods

Protein preparation

Constructs were generated by standard PCR-ligation techniques and sequences verified by automated sequencing. All proteins are from human unless specified. $BIRC3_{541\text{-}C}$ variants, $BIRC7_{239\text{-}C}$, full-length BIRC7 variants, $RNF2_{1\text{-}114}$ and $MDM2_{428\text{-}C}$ were cloned into pGEX4T1 (GE Healthcare) which contains an N-terminal glutathione S-transferase (GST) tag followed by a TEV protease cleavage site. $BMI1_{1\text{-}109}$ and $MDMX_{428\text{-}C}$ were cloned into pRSF_DUET (Novagen) which contains an N-terminal His-tag followed by a TEV protease cleavage site. Untagged UbcH5B variants were cloned into pRSF_1b vector. Proteins were expressed in *E. coli* BL21 (DE3) Gold. For crystallization, $BIRC7_{239\text{-}C}$ was purified by glutathione-affinity chromatography, treated with TEV protease to cleave the GST-tag, and further purified by desalting/glutathione-affinity pass-back and size exclusion chromatography. For ubiquitination assays, BIRC3 and BIRC7 variants were expressed and purified as described previously except cleavage was performed on glutathione sepharose beads and the pass-back step omitted. For Biacore analyses, GST-tagged $BIRC3_{541\text{-}C}$, $BIRC7_{239\text{-}C}$, full-length BIRC7 variants were purified by glutathione-affinity; GST-$MDM2_{428\text{-}C}$–His-$MDMX_{428\text{-}C}$ and GST-$RNF2_{1\text{-}114}$–His-$BMI1_{1\text{-}109}$ were purified by Ni^{2+}-NTA chromatography followed by glutathione-affinity; UbcH5B variants were purified by cation exchange and size exclusion chromatography. For ubiquitination assays, mouse Uba1 was expressed from pET23d (Novagen), charged with GST-Ub with 5 mM $MgCl_2$ and 5 mM ATP for 2h at 4°C and purified by glutathione-affinity chromatography eluted with 20 mM DTT, followed by anion exchange chromatography; His-Ub and ^{32}P-Ub were prepared as described previously[3]. Ub variants were cloned into pGEX2TK and purified as

described previously. UbcH5B variants were purified by cation exchange chromatography; ^{32}P-SMAC comprising residues 56-C was expressed from pET23d containing a C-terminal Protein kinase A recognition sequence (RRAVS) and purified by Ni-NTA affinity chromatography followed by size exclusion chromatography. All protein concentrations were determined by Bradford assay[4] with bovine serum albumin as standard and Ub concentration was determined as described previously[5]. Proteins were stored in 25 mM Tris-HCl (pH 7.6), 0.15 M NaCl and 1 mM DTT or 25 mM HEPES (pH 7.0), 0.15 M NaCl and 1 mM DTT at -80°C.

Structural determination

The data were integrated with automated XDS[6] and scaled using the CCP4 program suite[7]. $BIRC7_{239–C}$–$UbcH5B_{RAS}$~Ub complex crystals belong to space group $P4_32_12$ with two molecules in the asymmetric unit. Initial phases of $BIRC7_{239–C}$–$UbcH5B_{RAS}$~Ub were obtained by molecular replacement with PHASER[8] using PDB 3EB6 (BIRC3 RING–UbcH5B complex) and PDB 3A33 (UbcH5B~Ub) as the search models, respectively. All models were built in COOT[9] and refined using CCP4, CNS[10] and PHENIX[11].

The structure of $BIRC7_{239-C}$–$UbcH5B_{RAS}$~Ub (Chains A-F) was refined at a resolution of 2.18 Å and the final model contained two copies of UbcH5B (Chain A residues 2-147 and Chain D residues 2-147), $BIRC7_{239-C}$ (Chain B residues 242-298 and Chain E residues 242-298), Ub (Chain C residues 1-76 and Chain F residues 2-76). Residues with poor sidechain electron density were built as Ala. Details of the refinement statistics are shown in **Table 2**. All figure models were generated using PYMOL (Schrödinger).

Single turnover kinetics of di-Ub formation

UbcH5B was charged in a buffer containing 50 mM HEPES (pH 7.5), 50 mM NaCl, 5 mM $MgCl_2$, 5 mM ATP, 1 mM DTT, 0.3 U ml^{-1} inorganic pyrophosphatase, 0.3 U ml^{-1} creatine kinase, 5 mM creatine phosphate, mouse UBA1 (2.5 μM), ^{32}P-Ub variant (130 μM) and UbcH5B (66 μM) for 15 min at 23 °C. Charging was stopped by incubating the reaction with 0.25 U apyrase (Sigma) and 30 mM EDTA for 5 min at 23 °C. Different amounts of UbcH5B~^{32}P-Ub variants were then added to a reaction containing 50 mM HEPES (pH 7.5), 50 mM NaCl, His-Ub (820 μM; final concentration) and $BIRC7_{239–C}$ or $BIRC3_{541–C}$ variants. Final E3 concentrations are indicated in **Supplementary Fig. 6a,f**. Reactions were quenched with 2X SDS loading buffer containing 200 mM DTT at 30 s, resolved by SDS-PAGE, dried and exposed to a phosphorimager. Under these conditions, less than 15% of UbcH5B~^{32}P-Ub variants were transferred to His-Ub, thus representing initial rate. In addition there was no observable autoubiquitination of $BIRC3_{541–C}$ variants and $BIRC7_{239–C}$. Di-Ub bands were quantified using ImageQuant (GE Healthcare). Control reactions lacking E3 at each UbcH5B~^{32}P-Ub variant concentration were performed for background subtraction during quantification. All reported kinetic parameters were determined by fitting at least two independent datasets to the Michaelis-Menten equation using SigmaPlot 8.0 (Systat Software Inc.).

References

1. Reverter, D. & Lima, C.D. Insights into E3 ligase activity revealed by a SUMO-RanGAP1-Ubc9-Nup358 complex. *Nature* **435**, 687-92 (2005).
2. Mace, P.D. *et al.* Structures of the cIAP2 RING domain reveal conformational changes associated with ubiquitin-conjugating enzyme (E2) recruitment. *J Biol Chem* **283**, 31633-40 (2008).
3. Dou, H., Buetow, L., Hock, A., Sibbet, G.J., Vousden, K.H. & Huang, D.T. Structural basis for autoinhibition and phosphorylation-dependent activation of c-Cbl. *Nat Struct Mol Biol* **19**, 184-92 (2012).
4. Bradford, M.M. A rapid and sensitive method for the quantitation of microgram quantities of protein utilizing the principle of protein-dye binding. *Anal Biochem* **72**, 248-54 (1976).
5. Bohnsack, R.N. & Haas, A.L. Conservation in the mechanism of Nedd8 activation by the human AppBp1-Uba3 heterodimer. *J Biol Chem* **278**, 26823-30 (2003).
6. Kabsch, W. Xds. *Acta Crystallogr D Biol Crystallogr* **66**, 125-32 (2010).
7. Collaborative Computational Project, N. "The CCP4 Suite: Programs for Protein Crystallography". *Acta Cryst.* **D50**, 760-763 (1994).
8. Storoni, L.C., McCoy, A.J. & Read, R.J. Likelihood-enhanced fast rotation functions. *Acta Crystallogr D Biol Crystallogr* **60**, 432-8 (2004).
9. Emsley, P. & Cowtan, K. Coot: model-building tools for molecular graphics. *Acta Crystallogr D Biol Crystallogr* **60**, 2126-32 (2004).
10. Brunger, A.T. *et al.* Crystallography & NMR system: A new software suite for macromolecular structure determination. *Acta Crystallogr D Biol Crystallogr* **54**, 905-21 (1998).
11. Adams, P.D. *et al.* PHENIX: building new software for automated crystallographic structure determination. *Acta Crystallogr D Biol Crystallogr* **58**, 1948-54 (2002).